Communication / Navigation Outage Forecasting System (C/NOFS) Science Plan

The C/NOFS Science Definition Team,
(O. de La Beaujardière, Editor)

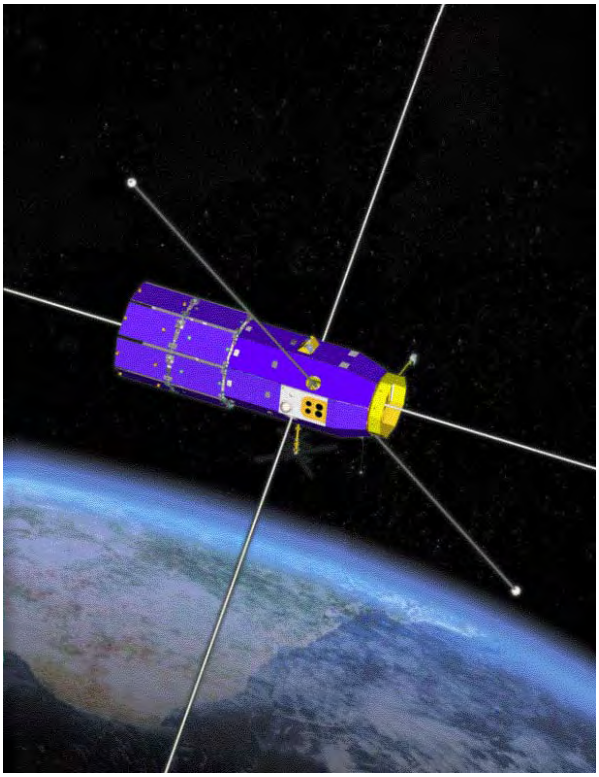

AIR FORCE RESEARCH LABORATORY
Space Vehicles Directorate
29 Randolph Road
Hanscom AFB, MA 01731-3010

This technical report has been reviewed and is approved for publication.

John B. Wissler, Lt Col, USAF
Chief, Battlespace Environment Division
Space Vehcles Directorate

Odile de La Beaujardière
Editor

Robert A. Morris, Chief
Space Weather Center of Excellence

This report has been reviewed by the ESC Public Affairs Office (PA) and is releasable to the National Technical Information Service (NTIS).

Qualified requestors may obtain additional copies from the Defense Technical Information Center (DTIC). All others should apply to the National Technical Information Service.

If your address has changed, if you wish to be removed from the mailing list, or if the addressee is no longer employed by your organization, please notify AFRL/VSIM, 29 Randolph Road, Hanscom AFB, MA 01731-3010. This will assist us in maintaining a current mailing list.

Do not return copies of this report unless contractual obligations or notices on a specific document require that it be returned.

Page intentionally left blank

C/NOFS Science Definition Team

Chair, C/NOFS Principal Investigator
Odile de La Beaujardière
Air Force Research Laboratory

C/NOFS Program Manager
Laila Jeong
Air Force Research Laboratory

Members
David Anderson
NOAA

John Ballenthin
Air Force Research Laboratory

Bamandas Basu
Air Force Research Laboratory

Santimay Basu
Air Force Research Laboratory

Theodore Beach
Air Force Research Laboratory

Paul Bernhardt
Naval Research Laboratory

William Borer
Air Force Research Laboratory

William Burke
Air Force Research Laboratory

Jorge Chau
Instituto Geofisico del Peru

Anthea Coster
MIT Haystack Observatory

Geoff Crowley
Southwest Research Institute

Dwight Decker
Air Force Research Laboratory

Bronislaw Dichter
Air Force Research Laboratory

Patricia Doherty
Boston College

Vincent Eccles
Space Environment Corporation

Bela Fejer
Utah State University

Cassandra Fesen
Dartmouth College

Keith Groves
Air Force Research Laboratory

Roderick Heelis
University of Texas at Dallas

Robert Holzworth
University of Washington

Cheryl Huang
Boston College

Joe Huba
Naval Research Laboratory

Donald Hunton
Air Force Research Laboratory

Dave Hysell
Cornell University

John Jasperse
Air Force Research Laboratory

Farzad Kamalabadi
University of Illinois

Michael Kelley
Cornell University

Linda Krause
U.S. Air Force Academy

Erhan Kudeki
University of Illinois

Jonathan Makela
Naval Research Laboratory

Frank Marcos
Air Force Research Laboratory

Nelson Maynard
Mission Research Corporation

Michael Mendillo
Boston University

John Meriwether
Clemson University

Evgenii Mishin
Boston College

Duggirala Pallamraju
Boston University

Larry Paxton
Applied Physics Laboratory

Robert Pfaff
NASA

John Retterer
Air Force Research Laboratory

Frederick Rich
Air Force Research Laboratory

Paul Rothwell
Air Force Research Laboratory

Joseph Salah
MIT Haystack Observatory

Robert Schunk
Utah State University

James Secan
Northwest Research Institute

Jan Sojka
Utah State University

Michael Starks
Air Force Research Laboratory

Paul Straus
Aerospace Corporation

Shin-Yi Su
Institute of Space Science, Taiwan

Roland Tsunoda
SRI International

Cesar Valladares
Boston College

James Whalen
Air Force Research Laboratory

Brian Wilson
Jet Propulsion Laboratory

Table of Contents

EXECUTIVE SUMMARY – C/NOFS SCIENCE PLAN 1
C/NOFS SCIENCE PLAN 2
1 Introduction 2
1.1 Document Road Map 2
2 C/NOFS Mission and Instruments 3
2.1 Core Components 3
2.1.1 Survey and Forecast Modes 4
2.1.2 Synergy with Other Agencies 4
2.2 C/NOFS Satellite Instruments 5
2.2.1 Ion and Electric Field Measurements 5
2.2.1.1 Planar Langmuir Probe (PLP) 5
2.2.1.2 Vector Electric Field Instrument (VEFI) 5
2.2.1.3 Ion Velocity Meter (IVM) 6
2.2.2 Neutral Winds 6
2.2.3 Total Electron Content 6
2.2.4 Ionospheric Scintillations 6
2.3 C/NOFS Ground-based Instruments 6
3 Background Ionosphere and Thermosphere 7
3.1 Irregularity Growth Rate 8
3.2 What are the Main Drivers of Equatorial Electric Fields? 10
3.2.1 Dynamo Electric Field 10
3.2.1.1 Past History of E-East 11
3.2.2 Post-Sunset Enhancement of Eastward Electric Field 12
3.2.2.1 Mechanism 1 12
3.2.2.2 Mechanism 2 13
3.2.2.3 Mechanism 3 13
3.2.2.4 Questions Related to Prereversal Enhancement 13
3.2.3 Role of Gravity Waves, Tropical Storms, and Lightning 14
3.2.3.1 Lightning as a Signature of Tropical Thunderstorms Which Can Cause Spread F 14
3.2.3.2 Lightning Electric Fields as a Direct Trigger for "Explosive" Spread F 15
3.2.3.3 Lightning Waveforms as a Local Plasma Diagnostic 15
3.2.3.4 GPS Occultation Observations of Stratospheric Gravity Waves 15
3.2.4 Role of Penetration Electric Fields 15
3.2.4.1 Post Midnight Bubbles during Magnetic Storms 16
3.2.4.2 Role Of High Latitude Field-Aligned Currents 17
3.2.5 Longitudinal Ionospheric Correlation Length 17
3.2.6 Separating Time and Longitude Effects 17
3.3 First-Principle Models of the Ambient Ionosphere 17
3.3.1 C/NOFS Assimilation Model 18
3.3.1.1 Electric Field Assimilation 18
3.3.1.2 Ion Density Assimilation 19
3.3.1.3 Thermospheric Assimilation 19
3.3.1.4 Assimilation of GPS Occultation Data 19
3.3.2 Ionospheric Forecasting 20
3.3.2.1 Ambient Forecast Model 20
3.3.3 Global 3D Modeling Using SAMI3 21
4 Triggering and Suppressing Equatorial Plasma Instabilities 22
4.1 Role of Wind Shear and Vertical Wind Variations 22
4.2 Effects of Plasma Inhomogeneities 22
4.3 Linear Growth Rate Model 23

4.4 Cascading Processes ... 24
4.5 What is the Bubble Spatial Structure? ... 25
5 Spread-F Irregularities ... 26
5.1 Overview and Examples ... 26
5.1.1 Fresnel and Bragg Scattering ... 27
5.1.2 Direct Observations ... 27
5.1.2.1 The San Marco Satellite ... 27
5.1.2.2 Sounding Rockets ... 30
5.2 Characterization of Irregularities That Cause Spread F ... 33
5.3 Using *In Situ* Wave Measurements to Test C/NOFS Predictive Models ... 35
6 Calculating Scintillation Indices from the C/NOFS Data ... 35
6.1 Phase Screen Theory ... 35
6.2 C/NOFS Phase Screen Algorithms ... 36
6.3 Phase Screen Science Issues ... 37
7 Develop Improved Scintillation Climatology ... 38
7.1 Seasonal Effects ... 39
7.2 Bottomside Sinusoidal Irregularities ... 39
7.3 Explain and Quantify Day to Day Variability ... 40
7.4 Solar Cycle Variability ... 41
7.5 Test of Simple Threshold Formulas to Nowcast and Forecast Scintillations ... 41
8 C/NOFS Instrument Development ... 42
8.1 Detection of Weak Equatorial Electric Fields ... 42
8.2 Magnetometer Data ... 43
8.3 Can the CORISS GPS Receiver Be Used for Scintillation Remote Sensing? ... 43
9 Coordinated Ground-Based Measurements ... 43
9.1 Jicamarca and Altair Radars ... 44
9.1.1 ISR Contributions Toward Operational Ionospheric Forecasting Systems ... 45
9.1.2 Altair ... 45
9.1.3 Jicamarca Radio Observatory ... 45
9.1.4 Other Ground-Based Instruments in South America ... 47
9.1.5 Pacific Sector ... 49
9.1.6 UHF and GPS Receivers for TEC and L-Band Scintillation Measurements ... 50
9.2 Instruments under Development ... 50
9.2.1 Special Ionosonde For Low Plasma Densities ... 50
9.2.2 Daytime FPI Measurements ... 50
9.2.3 Ground-Based Daytime Optical Airglow Studies ... 51
9.2.4 Tomographic Radio Receiver Array ... 51
10 Observation Campaigns ... 52
10.1 Ground-based Campaigns ... 52
10.2 Rocket Campaigns ... 52
10.3 Corroborative Satellite Observations ... 53
11 Conclusions ... 56
References ... 58
Acronyms ... 63

Illustrations

Figure 1. Artist's view of the C/NOFS project. C/NOFS scientists will use its extensive satellite and ground-based observations to conduct a program of focused theoretical investigations, collaborative measurements, and data analysis. 3

Figure 2. Engineering concept for the C/NOFS satellite showing the payload elements. 4

Figure 3. Map of existing and planned SCINDA ground stations which are scattered around the Earth's equatorial belt. Additional stations scheduled for installation will provide critical near real-time scintillation measurements for the C/NOFS program. These measurements will enable specification of the current scintillation environment, as well as constrain and enhance the predictions of the forecast algorithms. 7

Figure 4. Schematic of the formation of the latitude variation of ionization density in the equatorial F region, known as the equatorial (Appleton) anomaly. The diagram illustrates that during daytime the eastward dynamo electric field from the E region maps along the magnetic field to F-region heights above the magnetic equator. The plasma moves upward due to **E x B** drift and then diffuses along the magnetic field to form two crests with maximum ionization density near ±15° magnetic latitude and minimum ionization at the magnetic equator. 8

Figure 5a. (a) Schematic diagram of the plasma analog of the hydrodynamic R-T instability in the equatorial geometry. (b) Sequential sketches from photos of the hydrodynamic R-T instability. A lighter fluid initially supports a heavy fluid. 9

Figure 5b. Plasma instabilities observed at Jicamarca, Peru, on October 22, 1996. 10

Figure 6. Simplified model of the F-region prereversal enhancement of the zonal electric field. The neutral wind blows across the terminator generating a vertical electric field, which is no longer shorted out. This field maps along **B** to an equator-ward electric field in the E layer and tends to drive a westward current on both sides of the terminator. If no current flows in the nightside E region, a negative polarization charge builds up near the terminator, creating the zonal electric field E_ϕ. This E_ϕ maps back to the F region. 11

Figure 7. Superimposed plots of a large number of individual 24-hour measurements of vertical drifts at Jicamarca, Peru, showing the post-sunset or the prereversal enhancement of the eastward electric field. Data correspond to equinox solar maximum conditions for extended magnetic quiet (lower plot) and disturbed (upper plot) periods [From *Fejer et al.*, 1999]. 12

Figure 8. Dst measured near the times of two magnetic storms in (a) March 1989 and (b) March 1991 for 11 days roughly centered on the storm's maximum epoch. Vertical lines mark times of DMSP satellite encounters with EPBs. Light dotted lines, dashed lines, and heavy solid lines indicate increasing depletion severity [*Huang et al*., 2001]. 16

Figure 9. The satellite provides only a one-dimensional sampling of the parameters we need to specify in the 3D volume of the Earth's ionosphere. To alleviate this problem, several physical assumptions and simplifications must be made. 18

Figure 10. The C/NOFS ambient ionosphere forecast model. Models for several constituents of the ionosphere/thermosphere system are coupled to provide a forecast. 21

Figure 11. Plasma density obtained from the assimilation of observed vertical drifts into the low-latitude ionosphere model. The September 22, 1971 data are plotted as a function of altitude (km) and local

time. Superimposed on the plot are the contours of R-T growth rate spaced at increments of 2.5×10^{-4} s^{-1}, beginning with the outermost contour for a growth rate of 7.5×10^{-4} s^{-1}, and increasing inward. ... 23

Figure 12. Haleakala all-sky camera (ASC) image and GPS scintillations. Severe scintillations, as shown in the lower panel by the S4 index from the GPS data, correlate to depleted regions of electron density (upper panel). S4 index history shows scintillations occurred before the camera was turned on at 2020 LT. The GPS orbit is shown on the ASC image. 25

Figure 13. Data from the San Marco satellite showing plasma depletion in the bottom plot with associated radial and zonal DC electric fields in the next two plots. Plasma drifts associated with these electric fields are shown in the fourth plot from the bottom. The top plot shows the wave electric fields within the density depletion. Note that the wave electric fields are strongest where the DC electric fields are strongest, which, in this case, corresponds to regions near the edges of the plasma depletion. 28

Figure 14. Raw DC-coupled electric field data for the event shown in Figure 13 plotted with the filtered electric field data in the 0.4 – 4 Hz band. The filtered data show strong wave activity associated with km-scale structures. The large sine wave in the raw data is due to the spin of the San Marco satellite and is 90° out of phase between the two perpendicular electric field components. The amplitude of the large sine wave is mostly due to V x B which is primarily in the radial direction. By comparing the times when the amplitude of the filtered data maximizes with the peaks of the raw DC coupled waveforms, it is shown that the waves include a significant component in the radial direction. 29

Figure 15. Sounding rocket data from Kwajalein Atoll gathered in the presence of a strong spread-F event. The bottom plot shows the plasma density structure and a large depletion near 515 seconds flight time. The middle plot shows one component of the raw AC electric field data associated with the depletion in the passband of 15 -625 Hz. The top plot is a spectrogram of the AC electric fields. Note that the irregularity spectrum broadens in the region of the plasma density depletion. 30

Figure 16. A spectrum of the waves in the plasma density depletion at 515.5 seconds shown in Figure 15. Note the spectral peaks near 50 Hz and 1500 Hz, corresponding to tens of meters and tens of centimeters, respectively. Note that the rocket velocity, which was used to estimate the scales associated with the spectral peaks, is considerably less than that of an orbiting satellite. The AC electric field data shown here underwent a high pass filtering with a 3 dB point at 15 Hz. 31

Figure 17. Detailed spectral analysis of AC electric field and plasma density waveforms (top two plots) gathered on a second rocket flight from Kwajalein. The spectra of the density and electric field data are shown below the time series data and reveal similar spectral features for long and medium scale lengths. However, for shorter scale plasma waves < ~50 meters, the density spectrum is much steeper than the electric field spectrum. The lower plot shows the ratio of the two spectra and demonstrates how their spectral features diverge at shorter scales. Figure adapted from *Hysell* et al., [1994]. 32

Figure 18. Determination of the direction of the wave vector, k, and conversion of the measured satellite frame frequencies to wavelengths from the measured wave electric field vector, ΔE. See Section 5.2 for details. 33

Figure 19. Algorithm for scintillation estimation. Step 1: C/NOFS satellite measures ionospheric density perturbations and returns data to the ground. Step 2: Software is used to estimate the power spectrum of the density irregularities at a given location to help construct a 3D irregularity model for the local ionosphere. Step 3: A thin phase screen is constructed from the irregularity model for a given transmitter-receiver link, converting the geometry to an equivalent zenith screen. Step 4: A signal is propagated through the phase screen to produce a scintillating waveform characteristic of what would be received on the ground. Step 5: Statistics are gathered to determine the estimated strength of amplitude scintillation (S4) seen by a typical receiver..... 36

Figure 20. Distributions of EPB encounters as a function of the Kp index. The figure illustrates that the probability of encountering a plasma bubble increases with magnetic activity when Kp > 5. (a) Solid lines plot the number of equatorial crossings while Kp was in a given range. Dashed lines indicate the number of equatorial crossings when EPBs were detected. (b) Histograms give the percent of equatorial crossings during which EPBs were observed while Kp was in a given range [*Huang et al.*, 2001]. 40

Figure 22. Altair and Jicamarca incoherent scatter radars. 44

Figure 23. The two tables list the height and parameters that can be obtained from each of the Jicamarca radar operating modes. 46

Figure 24. 50 MHz radar interferometer results obtained on September 26-27, 1994 at the Jicamarca Radio Observatory, Peru, near the magnetic equator indicating the distribution of 3-meter irregularities along with their color-coded zonal drifts. The blue colors denote westward drift and red colors indicate eastward drift (*Kudeki et al.*, private communication); for description see *Basu et al.*, [1996]. 47

Figure 25. Site locations and field-of-view (40° elevation) of the GPS receivers used to obtain the latitudinal distributions of TEC. The GPS receivers at Bogotá, Iquitos, Pucallpa, Ancon, and Cuzco are operated by Boston College. The receivers at Iquique, Copiapo, and Antuco are part of the SAP (South Andes Project) network and are managed by the University of Hawaii. The receivers at Arequipa and Santiago form part of the IES network [*Valladares et al.*, 2001]. 48

Figure 26. The two plots show 3D views of the TEC values displayed as a function of geographic latitude and local time. TEC values were collected by the chain of GPS receivers in 1998. The top plot corresponds to a night when scintillations were seen at Ancon. The bottom plot is for a night of no scintillations [*Valladares et al.*, 2001]. 48

Figure 27. Images taken by two cameras atop the Haleakala volcano in Maui, showing the equatorial ionosphere visible from this site. The lower image is from a narrow-field camera set up to look tangent to field lines at the height of the airglow layer. 49

Figure 28. Examples of EPBs observed on DMSP. Plots show ion density (cm^{-3}) as a function of latitude at 20:00 MLT. Several levels of depletions are shown labeled M-0 to M-3 [*Huang et al.*, 2001]..... 54

Figure 29. Comparison of GUVI limb profiles with the predictions of the RIBG model. Each individual panel consists of the altitude axis shown horizontally. 54

Acknowledgements

The C/NOFS Mission is a joint effort of the DoD Space Test Program, AFRL, NASA, and NRL. AFRL gratefully acknowledges partial support for C/NOFS from AFOSR. We particularly thank the members of the C/NOFS Science Definition Team who so generously shared their knowledge and expertise during the development of this Science Plan. We are indebted to J. M. Campbell and L. C. Gentile from the Boston College Institute for Scientific Research for their dedication and attention to detail in preparing and editing this document. We also thank our colleagues at the Massachusetts Institute of Technology Haystack Observatory and the University of Massachusetts Lowell for their hospitality during the CNOFS Science Definition Team meetings.

EXECUTIVE SUMMARY – C/NOFS SCIENCE PLAN

This document describes the science to be conducted as part of the Communication / Navigation Outage Forecasting System (C/NOFS) Mission of the Air Force Research Laboratory. The primary component of the C/NOFS Mission is a satellite scheduled to be launched in January 2004 into a low inclination (13°) elliptical (~ 400 x 700 km) orbit. Ground-based instruments are also critical to the mission. The main purpose of C/NOFS is to forecast the presence of ionospheric irregularities that would adversely impact communication and navigation systems. The C/NOFS science team will exploit the extensive satellite and ground-based observations to conduct a program of focused theoretical investigations, collaborative measurements, and data analysis.

The C/NOFS science objectives can be organized into three broad categories:

1. Understand the physics of the ionospheric plasma in the equatorial regions at all local times, but with special emphasis on the post-sunset times, to forecast accurately the background ionosphere and the subsequent formation of scintillation-producing irregularities.

2. Understand the physical processes that lead to the formation of plasma bubbles and plumes in the ionosphere and identify the mechanisms that trigger or inhibit plasma instability.

3. Model the propagation of radio waves through the irregular equatorial ionosphere, in order to estimate the phase and amplitude scintillation, at all local times, longitudes, and for all frequencies.

This report discusses these objectives in more detail, provides the scientific rationale for necessary research, and describes the approach to reach these goals. The prospects for scientific achievement are substantial. Even after several decades of theoretical and experimental investigations, interpreting observations in the equatorial ionosphere and reliably forecasting scintillation strength still remain major scientific challenges.

C/NOFS is the first satellite solely dedicated to forecasting ionospheric irregularities and radio wave scintillations. It will be equipped with sensors that measure the following parameters: ambient and fluctuating electron densities; ion and electron temperatures; AC and DC electric fields; magnetic fields; neutral winds; ionospheric scintillations; and electron content along the lines of sight between C/NOFS and GPS satellites. Thus, the sensor suite on C/NOFS is richer than on any previously flown equatorial satellite. A broad range of ground-based measurements will complement the space data. In addition, data from several other satellites and rocket experiments will augment the C/NOFS observations. Several campaigns are planned to validate operational forecasts, acquire data to achieve the science goals, and test the theoretical models.

It is expected that the research will be done in collaboration with other government agencies including NASA, NSF, AFOSR, and ONR. Furthermore, the research will also include several international collaborations. Thus, one goal of this document is to begin the organization of a broader C/NOFS science team that involves the entire equatorial ionosphere research community.

We anticipate that at the end of the C/NOFS mission, our understanding of the physics of the equatorial ionosphere will have advanced to the point that we will be able to nowcast and forecast the formation of ionospheric irregularities with greatly improved accuracy. Thus, the science efforts will transition seamlessly to Space Weather applications.

C/NOFS SCIENCE PLAN

1 Introduction

The purpose of this document is to describe the scientific research to be conducted as part of the C/NOFS (Communication / Navigation Outage Forecasting System) Mission. A low-inclination (13°) elliptical (~ 400 x 700 km) satellite and ground-based instruments constitute the C/NOFS program.

C/NOFS will exploit extensive satellite and ground-based observations along with a program of focused theoretical investigations and data analysis to improve our understanding of the generation mechanisms of plasma turbulence in the nighttime equatorial ionosphere. As a byproduct, it will provide a forecast and nowcast of electron density profiles (EDPs) in the equatorial regions.

Plasma turbulence in the nighttime equatorial ionosphere is of considerable importance because scintillations caused by density irregularities result in outages of the communication and navigation systems that depend on trans-ionospheric radio links. The C/NOFS operational objective is to use the satellite and ground-based data to provide reliable forecasts of the time, location, and magnitude of the outages to Air Force (AF) users. The scientific objectives of the mission are described in this document.

The scientific objectives fall into three categories: (1) to understand the physical processes that determine the ambient ionosphere and thermosphere and that lead to plasma instabilities; (2) to identify mechanisms that trigger or quench the plasma irregularities responsible for signal degradation; and (3) to determine how the plasma irregularities affect the propagation of electro-magnetic waves.

An improved understanding of the physics of the ionospheric plasma and the upgraded models to describe it is essential for interpreting observations and for making reliable forecasts. Even after decades of theoretical and experimental investigations, interpreting the observations in the equatorial ionosphere and using them to make reliable forecasts of ionospheric activities remain major scientific challenges in the forefront of basic research.

1.1 Document Road Map

This document is organized by the general science goals that are needed to achieve the C/NOFS objectives. We will first describe the C/NOFS mission and instruments, then address the scientific questions related to the ambient ionosphere and neutral atmosphere. We next consider the formation and quenching of irregularities and the transmission of radio waves through the perturbed ionosphere. The following section deals with the coordinated ground and space observations, and the conclusions are summarized in the last section.

Throughout this document, we use a bold, italic font to indicate the scientific questions that could be resolved using data from the C/NOFS Mission.

2 C/NOFS Mission and Instruments

The C/NOFS mission will demonstrate state-of-the-art ionospheric disturbance forecasting and nowcasting, develop the means to improve those forecasts, and investigate the system impact of ionospheric scintillations. C/NOFS will thereby direct future scintillation product development.

Scintillations are random fluctuations in signal phase and amplitude that develop when radio waves pass through ionospheric electron density irregularities as they propagate to a receiver. As illustrated in Figure 1, scintillations degrade the performance of communication, navigation, and surveillance systems that rely on trans-ionospheric propagation. The science mission of the C/NOFS program is to improve understanding of equatorial spread F (ESF) disturbances and their associated radio wave scintillations with the goal of improving ionospheric scintillation forecasts. This is a broad mission that encompasses the specification and forecast of ion density, winds, electric fields, and plasma irregularities as well as the propagation of RF waves.

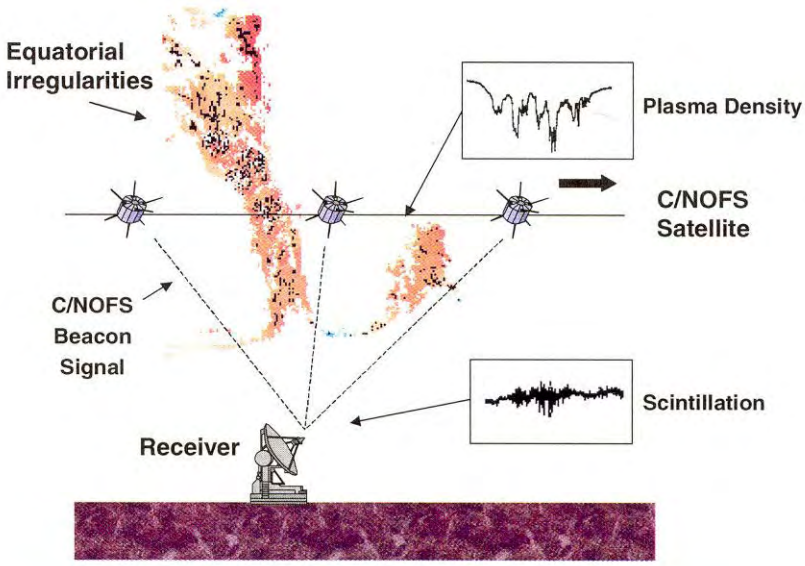

Figure 1. Artist's view of the C/NOFS project. C/NOFS scientists will use its extensive satellite and ground-based observations to conduct a program of focused theoretical investigations, collaborative measurements, and data analysis.

2.1 Core Components

The C/NOFS Mission consists of three core components: (1) a dedicated low-altitude, low-inclination satellite instrumented to monitor the equatorial ionosphere continuously around the globe, (2) a network of ground receivers to monitor scintillation conditions, and (3) the C/NOFS Data Center where data from the space- and ground-based sensors are combined to generate forecasting and nowcasting products.

The sensors on the C/NOFS satellite will provide information required to drive global ionospheric forecasts. C/NOFS will orbit the earth between 400 and 700 km in altitude at 13° inclination. This orbit keeps the satellite on magnetic field lines with apex altitudes of ≤ 800 km approximately half the time, and within the ionospheric equatorial anomaly regions for most of its orbit.

The satellite payload, which is described in more detail below, includes five sensors and a multi-frequency beacon (see Figure 2). A unique aspect of the space mission is that during the later stage, data from the sensors (along with some satellite telemetry) will be relayed in real time through NASA's Tracking and Data Relay Satellite System (TDRSS).

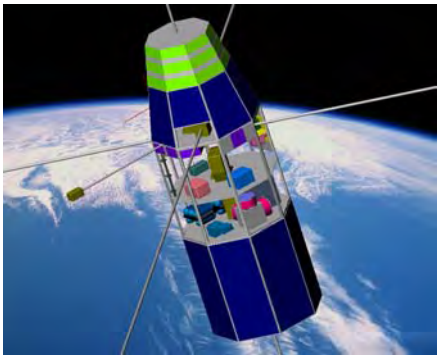

Figure 2. Engineering concept for the C/NOFS satellite showing the payload elements.

2.1.1 Survey and Forecast Modes

The C/NOFS satellite mission has two phases, Survey Mode and Forecast Mode. During Survey Mode the C/NOFS sensor suite will collect as much data as possible to identify the key parameters for predicting scintillations. Survey Mode data will be used to validate models and forecasting tools developed prior to launch. C/NOFS will operate in Survey Mode for the first nine months of the mission, then transition to Forecast Mode for the remainder of the first year of payload operations. During Forecast Mode, selected instrument data will be down linked in real time to demonstrate the prediction of scintillation events based on the models tested during Survey Mode.

Two additional years of on-orbit operations are planned for the C/NOFS mission. During this time, the satellite will support a prototype operational demonstration of the ability to forecast scintillation events and to provide usable communication / navigation outage warnings to affected users. Operations in Forecast Mode beyond one year will also allow time to improve prediction algorithms. The satellite will function in Forecast Mode for most of this mission phase.

The five instruments and tri-band beacon that comprise the C/NOFS satellite payload are classified into four groups, depending on the measurements that they perform or relate to: (1) Ions and Electric Fields, (2) Neutral Winds, (3) Total Electron Content, and (4) Ionospheric Scintillations. Together, the C/NOFS instruments will provide the comprehensive measurements required for mission success under all orbital conditions.

2.1.2 Synergy with Other Agencies

Although the demonstration of an operational scintillation forecast system will be carried out by the Air Force Research Laboratory Space Vehicles Directorate (AFRL/VS), the C/NOFS science mission is a multi-agency mission. The satellite observations will be augmented by data from several National Science Foundation (NSF) facilities as well as other ground-based and satellite instruments. At this time, it is anticipated that other agencies such as NSF, the National Aeronautics and Space Administration (NASA), the Air Force Office of Scientific Research (AFOSR), and the Office of Naval Research (ONR) will leverage and complement the AFRL C/NOFS program. Both

experimental and theoretical efforts are planned to be funded as a C/NOFS Guest Investigator / Ground-Based Augmentation Program.

2.2 C/NOFS Satellite Instruments

Table 1 lists the satellite instruments, the principal investigators, and their institutions.

Table 1. C/NOFS instruments and principal investigators.

Name	Instrument	Measured Parameters	PI and Organization
PLP	Planar Langmuir Probe	- Ion density - Electron temperature - Power spectral densities	D. Hunton AFRL
IVM	Ion Velocity Meter	- Vector ion drift velocities - Ion temperature - Ion composition	R. Heelis U. Texas at Dallas
NWM	Neutral Wind Meter	- Vector neutral wind velocities - Neutral composition	G. Earle U. Texas at Dallas
VEFI	Vector Electric Field Instrument	- Vector DC & AC electric fields - Magnetic fields - Relative plasma density - Optical lighting emission	R. Pfaff NASA GSFC
CERTO	Coherent Electromagnetic Radio Tomography	- Space-to-ground scintillations - Ne reconstruction	P. Bernhardt NRL
CORISS	C/NOFS Occultation Receiver for Ionospheric Sensing and Specification	- Ne profiles - Line-of-sight TEC - Space-to-space scintillation - Stratospheric refractivity	P. Straus Aerospace Corp.

2.2.1 Ion and Electric Field Measurements

2.2.1.1 Planar Langmuir Probe (PLP)

The Planar Langmuir Probe (PLP) is a dual disk probe to sense ionospheric plasma density. PLP provides low time-resolution density inputs for ionospheric modeling and high time-resolution measurements of density irregularities for disturbance microphysics. The electron density and temperature will be used to quantify the conditions that produce scintillations and to model EDPs. PLP also monitors the spacecraft surface potential.

2.2.1.2 Vector Electric Field Instrument (VEFI)

The Vector Electric Field Instrument (VEFI) consists primarily of three orthogonal 20-m tip-to-tip double probe antennas. VEFI measures DC electric fields that cause the bulk plasma motion that drives the ionospheric plasma unstable. Additionally, it measures the quasi-DC electric fields within the plasma density depletions to reveal the motions of the depletions relative to the background ionosphere. VEFI also measures the vector AC electric fields which characterize the microphysics of ionospheric disturbances associated with spread F irregularities. A fluxgate magnetometer, optical lightning detector, and fixed-bias Langmuir probe are also included in the VEFI instrument package.

2.2.1.3 Ion Velocity Meter (IVM)

The Ion Velocity Meter (IVM) consists of two sensors, an ion drift meter (IDM) and a retarding potential analyzer (RPA) that will directly measure the ion drift vector, the ion temperature, and the major ion composition with a spatial resolution of ~4 km along the satellite track. The IDM will also provide measurements of the local vertical and horizontal ion drift components with a spatial resolution of 500 m.

2.2.2 Neutral Winds

The Neutral Wind Meter (NWM) comprises two sensors, a cross track wind sensor (CTS) and a ram wind sensor (RWS) that will directly measure the neutral wind vector with a spatial resolution of ~8 km along the satellite track. Measurements will be made over a restricted altitude range between perigee and the exobase, which is dependent on solar activity levels during the mission.

The IVM and NWM instruments on C/NOFS will also be used to conduct the Coupled Ion Neutral Dynamics Investigation (CINDI) sponsored by NASA. This collaborative endeavor between the Air Force and NASA is designed to maximize the science and operational capabilities of the instrumentation.

2.2.3 Total Electron Content

The C/NOFS Occultation Receiver for Ionospheric Sensing and Specification (CORISS) is a Global Positioning System (GPS) dual-frequency receiver. CORISS measures total electron content (TEC) along the line-of-sight between C/NOFS and GPS satellites, thus providing a remote sensing technique for vertical profile information during occultations (i.e., when GPS satellites are setting). Limb profiles of TEC can be inverted to produce vertical profiles of electron density. CORISS TEC measurements from occulting and non-occulting GPS satellites at various bearings relative to the satellite track constrain C/NOFS ionospheric models. It is also possible to measure L-band scintillations caused by electron density irregularities on lines-of-sight between C/NOFS and GPS satellites. This technique is currently in an early stage of development.

2.2.4 Ionospheric Scintillations

The Coherent Electromagnetic Radio Tomography (CERTO) is a tri-band (150 MHz, 400 MHz, 1067 MHz) radio beacon. CERTO is used for multi-frequency scintillation studies with ground receivers (measurement in the region between the C/NOFS satellite and the Earth). CERTO will also be used for tomographic reconstruction of EDPs.

2.3 C/NOFS Ground-based Instruments

On the ground, the scintillation receivers for C/NOFS constitute the Scintillation Network Decision Aid (SCINDA). SCINDA sites have been established at Ancon, Peru; Antofagasta, Chile; Ascension Island; Bahrain; Diego Garcia; Guam; Manila, Philippines; and Singapore, as shown in Figure 3. The SCINDA sites have small, simple receivers that monitor beacon signals from geostationary satellites to determine the amplitude scintillation index (S_4), which is relayed to the Data Center every 15 minutes. These receivers use spaced antenna measurements to provide an estimate of the drift of ionospheric irregularities. SCINDA sites also have GPS receivers to monitor amplitude and phase scintillations on all available GPS satellite links. Future upgrades include adding steerable antennas at selected sites to track the CERTO beacon signals from the C/NOFS satellite and incorporate GPS TEC measurements.

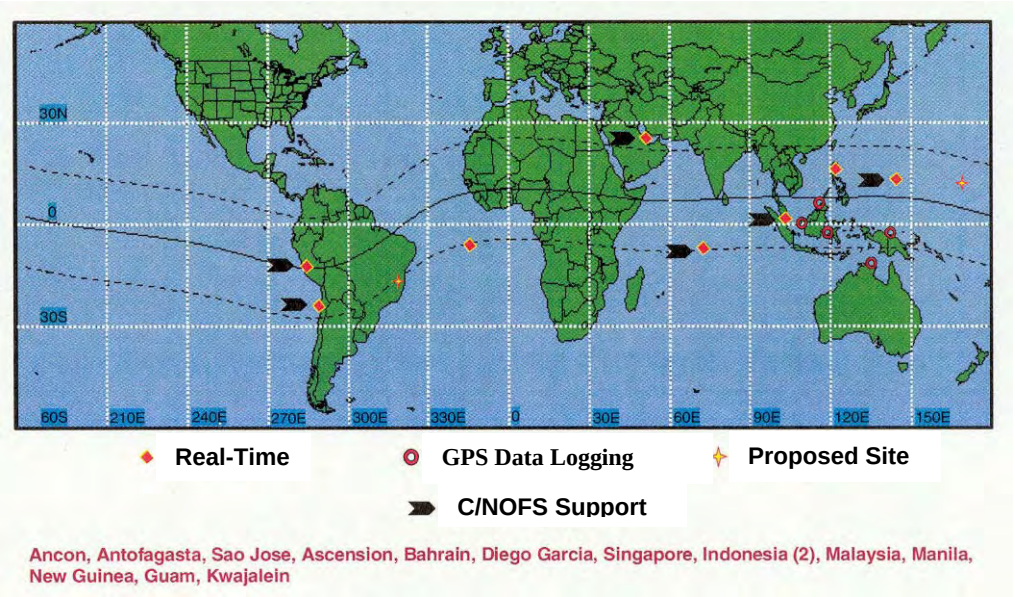

Figure 3. Map of existing and planned SCINDA ground stations which are scattered around the Earth's equatorial belt. Additional stations scheduled for installation will provide critical near real-time scintillation measurements for the C/NOFS program. These measurements will enable specification of the current scintillation environment, as well as constrain and enhance the predictions of the forecast algorithms.

3 Background Ionosphere and Thermosphere

In order to specify and forecast the onset of scintillations we must exploit the C/NOFS data to model the background ionosphere and thermosphere in which plasma irregularities grow. The morphology of the equatorial ionosphere is quite different from that at other latitudes because the magnetic field, **B**, is nearly parallel to the Earth's surface. During daytime, the E-region dynamo electric field (**E**) is eastward. An eastward electric field in the E region at off-equatorial latitudes maps along the Earth's magnetic field to F-region heights above the magnetic equator. As illustrated in Figure 4, the resulting **E** x **B** drift transports F-region plasma upward at the magnetic equator. The uplifted plasma then moves along **B** in response to gravity and pressure-gradient forces. As a result, the equatorial (Appleton) anomaly is formed with minimum F-region ionization density at the magnetic equator and maxima at the two crests approximately 15° to 20° in magnetic latitude to the north and south.

Near sunset, plasma densities and dynamo electric fields in the E region decrease, and the Appleton anomaly begins to fade. However, at this local time a dynamo develops in the F region. Polarization charges within conductivity gradients at the terminator enhance the eastward electric field for about an hour after sunset. The post-sunset electric field moves the ionospheric plasma upward, allowing the Appleton anomaly crests to intensify. Eventually the electric field turns westward, causing plasma to drift downward. Soon after sunset, vertical plasma density gradients form in the bottom side of the F layer. The upward density gradient is opposite in direction to the gravitational force. This configuration is Rayleigh-Taylor (R-T) unstable and allows plasma density irregularities to form. Eastward (westward) post-sunset electric fields enhance (quench) the R-T instability. On some days the magnitude of **E** is insufficient to cause equatorial anomaly crests or ionospheric irregularities before its polarity reverses.

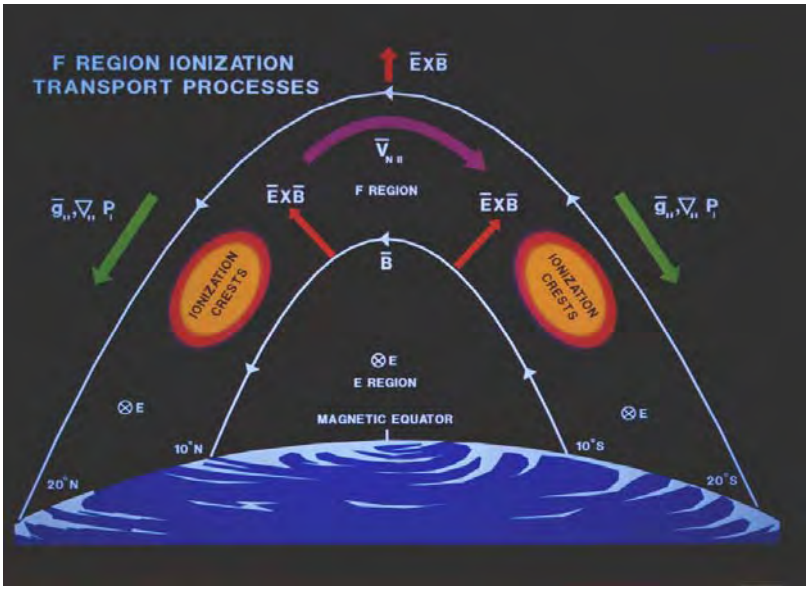

Figure 4. Schematic of the formation of the latitude variation of ionization density in the equatorial F region, known as the equatorial (Appleton) anomaly. The diagram illustrates that during daytime the eastward dynamo electric field from the E region maps along the magnetic field to F-region heights above the magnetic equator. The plasma moves upward due to **E x B** drift and then diffuses along the magnetic field to form two crests with maximum ionization density near ±15° magnetic latitude and minimum ionization at the magnetic equator.

3.1 Irregularity Growth Rate

After sunset, the E layer virtually disappears due to rapid recombination of ions and electrons and, as the recombination rates decrease with increasing altitude, a sharp upward density gradient develops on the bottomside of the F layer. The plasma on the bottomside is then driven unstable by the combined effect of gravity, eastward electric field, and vertically downward neutral wind velocity. The so-called 'bubbles' and 'plumes', which are observed in the nighttime equatorial ionosphere, are the fully developed nonlinear state of the density fluctuations (irregularities) resulting from the instability. The instability process is referred to as the collisional interchange instability or the generalized R-T instability [*Balsley et al.*, 1972*; Kelley*, 1989], which is illustrated in Figure 5. Figure 5a explains the instability mechanism and Figure 5b shows a dramatic example from the Jicamarca Radar in Peru.

The spatially inhomogeneous equatorial plasma is embedded in a dipole magnetic field. Since the R-T instability involves the interchange of entire magnetic flux tubes, spatial variations of ambient plasmas along the curved magnetic field lines have significant effects on the growth rates and topologies of the excited modes. Proper mathematical treatment of these effects requires solution of complicated partial differential equations [*Basu and Coppi*, 1983; *Basu*, 1998; *Basu*, 2002]. A somewhat simpler description that also takes into account the effects of plasma inhomogeneity along the field line, albeit in a gross manner, is the flux-tube integrated description introduced originally by *Haerendel* [private communication, 1973]. In this description, the relevant plasma equations are

integrated along equipotential field lines. Perturbation analysis is then applied to the flux-tube integrated equations to determine the linear growth rates.

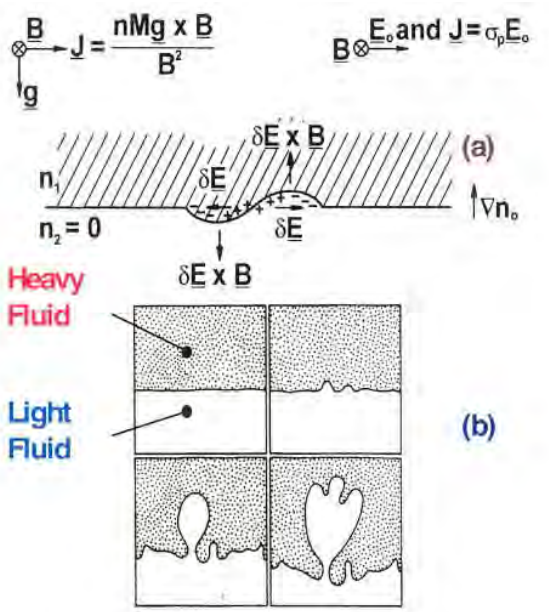

Figure 5a. (a) Schematic diagram of the plasma analog of the hydrodynamic R-T instability in the equatorial geometry. (b) Sequential sketches from photos of the hydrodynamic R-T instability. A lighter fluid initially supports a heavy fluid.

With some approximations, the linear growth rate γ for the flux tube integrated generalized R-T instability can be written as [*Sultan*, 1996]

$$\gamma = \frac{\Sigma_P^F}{\Sigma_P^E + \Sigma_P^F}\left(V_p + U_n^P + \frac{g_L}{\nu_{in}^{eff}}\right)\frac{1}{L_n} - R_T \qquad (1)$$

Here g_L is the <u>vertically downward</u> acceleration due to gravity g at the magnetic equator and on a field line designated by the L (McIlwain parameter) value, so that $g_L = g_0 / L^2$, where g_0 is the value on the surface of the earth (L = 1); $V_p = cL^3 E_0 / B_0$, where V_p is the <u>vertically upward</u> drift velocity due to the <u>eastward</u> electric field E_0 at the magnetic equator; B_0 is the value of magnetic field B on the surface of the earth (L = 1), U_n^P is the <u>vertically downward</u> neutral wind velocity perpendicular to the magnetic field that has been weighted by the Pedersen conductivity; ν_{in}^{eff} is the flux-tube integrated effective F-region ion-neutral collision frequency weighted by number density along the flux tube; L_n is the scale-length of the vertical gradient of the F-region flux-tube integrated plasma density measured at the equator; R_T is the flux-tube integrated recombination rate; and Σ_P^E and Σ_P^F are the contributions to the flux-tube integrated Pedersen conductivity from the E and F

regions, respectively. For the above specified directions of electric field, neutral wind velocity, and acceleration due to gravity, the growth rate γ of the R-T instability can be positive only when L_n is positive. The growth period, 1/γ, is of the order of 12 minutes, and it takes a few growth periods for a bubble to be fully formed. Since g and B are constants at a given L, the growth rates are controlled by the variability of $1/L_n$, E_0, U_n^P, Σ_P^E, Σ_P^F, ν_{in}^{eff}, R_T and by the height of the F layer, through the flux-tube integrated quantities.

That γ depends on the flux-tube integrated Pedersen conductivity, rather than just the local value near the magnetic equator, is important for understanding the seasonal variability of ESF occurrence at a given longitude. As we examine the influence of these parameters, keep in mind that the thermosphere and ionosphere are so closely coupled that it is somewhat arbitrary to classify them separately.

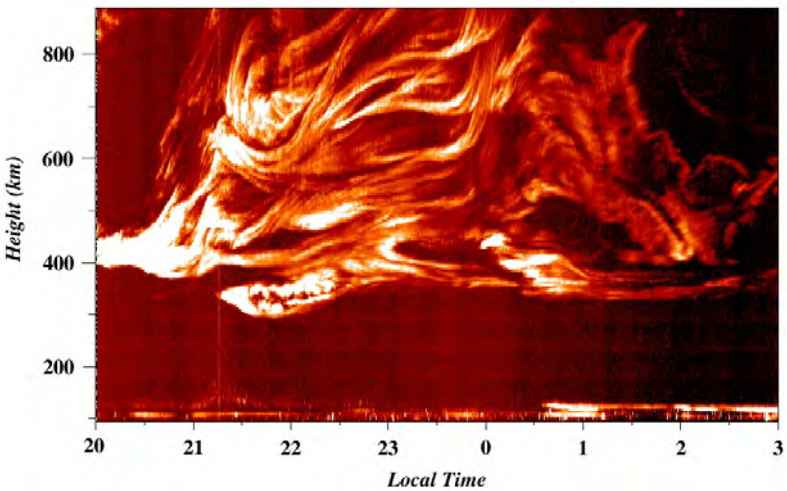

Figure 5b. Plasma instabilities observed at Jicamarca, Peru, on October 22, 1996.

3.2 What are the Main Drivers of Equatorial Electric Fields?

Equation (1) indicates the role of the acceleration due to gravity, the eastward electric field, and the downward neutral wind velocity in the R-T growth rate. The eastward electric field is especially important since it affects the growth rate in two ways: (a) it contributes directly to the growth rate, and (b) it moves the F layer vertically upward to higher altitudes where ν_{in}^{eff} is smaller, and thus enhances the value of the growth rate term associated with g. The height of the F layer at the magnetic equator after sunset is determined by the time history of the electric field, which is a global phenomenon. Electric fields have several possible sources. ***Using C/NOFS data, can we model these electric fields with enough precision to discriminate between their various sources?***

3.2.1 Dynamo Electric Field

The first source is the thermospheric dynamo that drives the equatorial electrojet [*Haerendel and Eccles*, 1992; *Eccles*, 1998a]. Extreme ultraviolet (EUV) radiation from the Sun creates ion-electron pairs in the lower ionosphere on the dayside and heats the thermospheric neutral atmosphere. Consequent neutral winds push plasma across magnetic field lines creating **U x B** electric fields,

where **U** is the neutral wind velocity. In crossing the day-to-night terminator, most plasma at low altitudes in the ionosphere is lost through recombination. Polarization electric fields are required to maintain current continuity across the steep conductivity gradient that develops along the terminator line. It is often assumed that these electric fields cause plasma to rise in the early post-sunset sector and fall in the later evening hours. The geometry of the fields, wind, and terminator is sketched in Figure 6.

In an idealized representation, F-layer plasma in the evening sector resembles a standing vortex. While the plasma is rising, the electric field is eastward and contributes to positive γ. Downward plasma motion at later local times, due to westward electric fields, contributes to ionospheric stabilization. An important aspect of the C/NOFS measurements is that the winds will be measured directly and will help establish the precision and validity of existing thermospheric models.

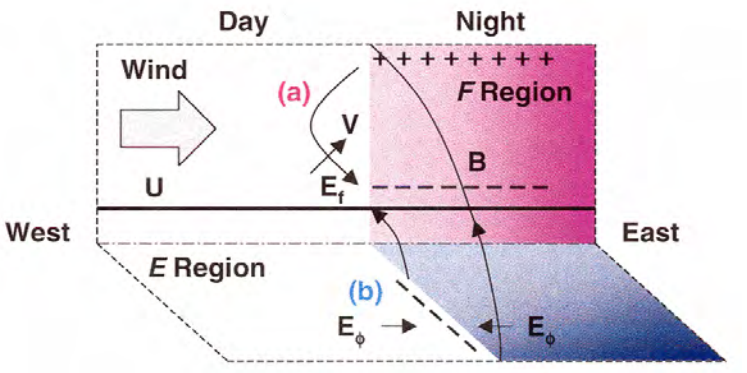

Figure 6. Simplified model of the F-region prereversal enhancement of the zonal electric field. The neutral wind blows across the terminator generating a vertical electric field, which is no longer shorted out. This field maps along **B** to an equatorward electric field in the E layer and tends to drive a westward current on both sides of the terminator. If no current flows in the nightside E region, a negative polarization charge builds up near the terminator, creating the zonal electric field E_ϕ. This E_ϕ maps back to the F region.

3.2.1.1 Past History of E-East

As noted above, the eastward electric field component has a subtle but extremely important controlling influence, far beyond its role in stabilizing or destabilizing the upward plasma gradient. The time history of E-East before, during, and just after sunset determines the height of the dense post-sunset plasma. After sunset, this plasma is no longer subject to the shorting-out effect of conducting E regions far to the north and south, but the growth rate is an exponentially increasing function of its height. In the linear approximation, an increase of ~50 km in altitude increases the instability growth time by a factor of e. It has been said that the single most important parameter controlling scintillations is the post-sunset altitude of the layer and, since E-East controls this height, knowledge of this parameter is crucial.

Will the C/NOFS wind and EDP measurements just before and after sunset allow a reliable forecast of scintillations? Is the EDP model derived from C/NOFS data useful in determining the height of the F layer and the scintillation probability?

3.2.2 Post-Sunset Enhancement of Eastward Electric Field

During daytime, the electric field is eastward and, therefore plasma drift is upward. The plasma drift reverses to the downward direction at ~19 LT. However, just before the drift reversal at the time of sunset, the eastward drift is much enhanced, as illustrated in Figure 7 [*Fejer et al.*, 1999]. This enhancement is called the post-sunset or the prereversal enhancement (PRE) of the eastward electric field. The PRE causes rapid uplifting of the F region, and steepens the bottomside gradient leading to the R-T instability. (The vertical uplift of the plasma layer by the eastward electric field helps in increasing the bottomside density gradient because the recombination frequency decreases exponentially with altitude as shown by Equation (24) in *Basu* [1997]. The R-T instability generates irregularities with scale sizes ranging from tens of kilometers to tens of meters. PRE holds the key to the formation of irregularities and, as such, the nowcasting and forecasting of irregularities and PRE are interrelated. ***What is the driver of the PRE and which parameters control its magnitude?*** Three main mechanisms have been proposed, as are briefly discussed below (see [*Eccles*, 1998b]).

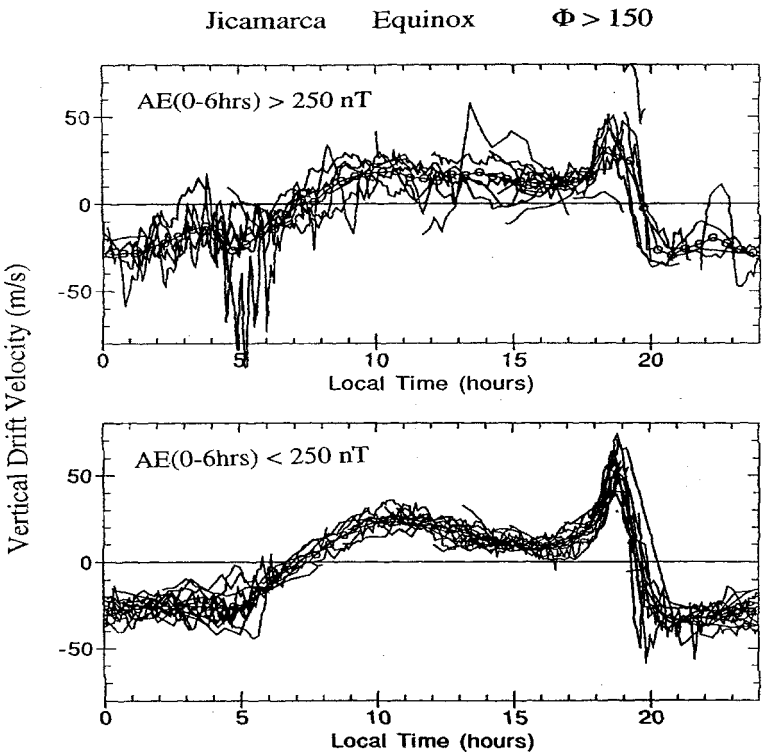

Figure 7. Superimposed plots of a large number of individual 24-hour measurements of vertical drifts at Jicamarca, Peru, showing the post-sunset or the prereversal enhancement of the eastward electric field. Data correspond to equinox solar maximum conditions for extended magnetic quiet (lower plot) and disturbed (upper plot) periods [From *Fejer et al.*, 1999].

3.2.2.1 Mechanism 1

The cause of PRE at sunset has been attributed to the charge collection in the off-equatorial E region where the Hall conductivity reduces rapidly with local time. As illustrated in Figure 6, the eastward component of the neutral wind in the F region causes a downward E field (- **U x B**). This E field is smaller on the dayside because of larger E-region conductivity to which it is connected by the

magnetic field. The electric field maps down to the E region and drives a westward Hall current in the E region. Because of the much-reduced Hall conductivity on the nightside, the Hall current is much larger on the dayside. This results in a collection of polarization charges near the terminator and creates an eastward electric field enhancement on the dayside of the terminator [*Farley et al.*, 1986].

Therefore, the conductivity of the ionosphere in magnetic contact with the unstable region is a critical quantity. In the laboratory, this is referred to as a conducting end plate, which stabilizes flute mode instabilities. However, this is a difficult measurement. It can be done from the ground using special ionosondes. Alternately, the CORISS instrument, which can measure relative E-region density peaks down to densities of ~5×10^3 cm^{-3}, may be able to make this conductivity measurement when the GPS occultation geometry permits. In addition, *Kelley* [1989] has shown that if the Poynting flux is measured in bubble regions, the end-plate conductivity can be measured during spread-F conditions. This might be possible using the electric and magnetic field sensors on C/NOFS.

3.2.2.2 Mechanism 2

In this case, the F-region dynamo is considered to be driving the vertical Pedersen current, and the electrojet supplies the current demanded by the F-region dynamo. The rapid drop of conductivity in the equatorial electrojet at sunset coupled with increased current demand of the F-region dynamo on the nightside requires an enhanced zonal electric field or PRE. The PRE draws the electrojet current zonally to meet the current demands of the F-region dynamo on the nightside. [*Haerendel and Eccles*, 1992].

3.2.2.3 Mechanism 3

It follows from the original paper on polarization electric fields [*Rishbeth*, 1971] that the polarization electric field suddenly develops at sunset due to the F-region dynamo. Because of the edge effect, the electric lines of force become curved. The plasma drifts that are normal to the electric lines of force converge at sunset to cause vertical plasma drift. Basically, this is a result of the curl free properties of the polarization electric field that changes abruptly across the sunset line [*Eccles*, 1998b].

3.2.2.4 Questions Related to Prereversal Enhancement

The F-region dynamo drives the PRE as it acts across the conductivity gradient caused by the sunset terminator.

Can we establish the relative timing of the west to east change of the F-region neutral wind and the terminator-induced conductivity gradient? How strong is the eastward zonal neutral wind needed at the time of sunset?

Since the F-region neutral wind is defined by tidal modes, is it possible to predict the behavior of the zonal neutral winds at the time of sunset from daytime patterns?

What is the relationship between the day-to-day variability of spread F with the variability of neutral wind tidal modes?

Nighttime neutral wind measurements by Fabry-Perot Interferometers assume that there is no vertical neutral wind to avoid the need for the absolute calibration of the wavelength of airglow emissions. Can we establish the presence of vertical neutral winds as they impact the growth rate of the R-T instability?

Because the CINDI instrument will provide the most accurate neutral wind observations ever obtained from a satellite – and these observations have been very sparse – the C/NOFS Mission, in conjunction with ground-based observations is expected to provide breakthrough results related to the role of the neutral winds in equatorial aeronomy.

3.2.3 Role of Gravity Waves, Tropical Storms, and Lightning

Gravity waves from the troposphere have long been considered an important source of energy transfer in the ionosphere/thermosphere system. A potential source of electric fields is plasma uplift in the post-sunset sector by gravity waves. The upward push due to these waves creates local zonal **U** x **B** currents alternatively east and west. These currents are not divergence-free and result in east and west electric fields. It has been suggested that gravity waves propagating in the neutral atmosphere could act as seeds for equatorial plasma bubbles (EPBs) [*Kelley et al.*, 1981; *Rottger*, 1981]. In this hypothesis, the postsunset ionosphere would be rising due to the thermospheric dynamo. Gravity waves would provide an extra push toward instability at a higher growth rate. *McClure et al.* [1998] argued that the global morphology of bubble occurrence suggests that tropospheric disturbances act as the main seeds for EPBs. Recently, *Prakash* [1999] developed a theoretical model that only requires gravity-wave winds to couple to the E-region altitudes. Electric fields associated with Hall, rather than Pedersen, currents couple to the F layer and thus provide the seeds for bubble formation. This model predicts that gravity wave sources are at low latitudes. Thus, meridionally propagating gravity waves from auroral disturbances cannot act as seeds for EPBs.

However, such gravity waves may be launched by tropical storm systems in the troposphere. To date, neither the correlation nor the causal link between tropical storms and spread F has been firmly established, although it is believed that gravity waves and their associated DC electric fields may provide the critical linkage between the two regions. Indeed, ionospheric electric field structures have been detected over regions of severe tropospheric storms on the San Marco [*Farrell et al.*, 1994] and Dynamics Explorer-2 [*Burke et al.*, 1992] satellites. Likewise, *Kelley* [1997] observed gravity-wave generation of ionospheric disturbances. The DC fields propagate at the speed of light to the ionosphere and last a few tens of milliseconds. Thus, it is not obvious that they could have an important effect on the linear growth with time scales of several minutes. How does this fit in with the explosive growth concept? Has the ionosphere already passed through several linear growth periods, then a kick sends it non-linear? ***The mechanism of upward energy propagation from tropical thunderstorms in initiating spread F must be established in order to develop a successful prediction model to meet the C/NOFS goals.***

Lightning-related electric fields associated with tropical storms in the troposphere, on the other hand, have been shown to be a definitive source of short-lived ionospheric irregularities called explosive spread F. The Lightning Detector (LD) on the C/NOFS VEFI instrument can distinguish the lightning-related electric fields that create such prompt ionospheric irregularities. Furthermore, the electromagnetic wave signature associated with lightning can be used as an effective diagnostic for determining local ionospheric plasma parameters below the C/NOFS satellite, as discussed below.

3.2.3.1 Lightning as a Signature of Tropical Thunderstorms Which Can Cause Spread F

The C/NOFS database will provide for the first time a means to establish a correlation between tropical storms and spread-F gravity waves launched from the storms and/or their associated DC electric fields. The C/NOFS LD will provide a signature of the storm activity to be used to establish the statistical correlations. We will examine in particular the neutral motions and possible enhanced background DC electric fields that may be associated with tropospheric storms. Data from NASA's Tropical Rainfall Measuring Mission satellite have shown that flash rates increase exponentially with storm height [*Ushio et al.*, 2001]. It is precisely these tall thunderstorms that are known to produce electron density perturbations in the ionosphere [*e.g. Kelley*, 1997], which in turn could stimulate spread F [*Rottger*, 1981]. The LD on C/NOFS will record such increased flash rates for examination in the context of observed and predicted spread-F ionospheric irregularities.

3.2.3.2 Lightning Electric Fields as a Direct Trigger for "Explosive" Spread F

Using Jicamarca incoherent scatter radar data, *Woodman and Kudeki* [1984] provided direct evidence for the explosive onset of spread F resulting from lightning. NASA rocket flights directly over thunderstorms have now demonstrated the dramatic effects of lightning on ionospheric plasmas in the same altitude region as C/NOFS [*e.g., Kelley et al.*, 1985; *Kelley*, 1989; *Li*, 1993; *Barnum*, 1999]. The mechanism for the energy deposition from lightning is under investigation, but the triggering itself is well documented. The C/NOFS mission is designed not only to monitor the occurrence of lightning-generated explosive spread F, but also to investigate the physical mechanism for the phenomenon. Lightning-related electric field waves originating as far away as 2500 km from the satellite sub-track can be detected by the VEFI instrument and captured optically by the LD [*Holzworth et al.*, 1999].

3.2.3.3 Lightning Waveforms as a Local Plasma Diagnostic

The VEFI LD provides a powerful tool for plasma diagnostics. In particular, using the LD signal as a trigger for capturing the VEFI electric field waveform allows direct measurement of the vertical TEC below the satellite. Such information will complement the TEC information obtained by other C/NOFS instruments, which cannot obtain the vertical TEC with high spatial resolution. Lightning, identified by the LD, produces a broadband electromagnetic signal that propagates through the earth-ionospheric waveguide and enters the lower ionosphere, converting to a plasma wave called a whistler mode wave nearly vertically through the ionosphere [*Helliwell*, 1965; *Li*, 1993; *Barnum*, 1999]. The dispersion of this signal is caused by the fact that whistler mode waves of different frequencies travel at different speeds. This dispersion gives a direct measure of the TEC through which the whistler wave propagated to reach the satellite. This method was first used at equatorial latitudes using rocket borne E field instruments.

Observations of this dispersion as C/NOFS moves through different altitudes can give the average electron density by taking the difference of the TEC seen from different altitudes. Knowledge of the TEC and local plasma density is critical information for the C/NOFS mission.

3.2.3.4 GPS Occultation Observations of Stratospheric Gravity Waves

CORISS provides another method of determining the presence of gravity waves generated by tropical storms. In addition to its primary function of providing ionospheric TEC measurements, CORISS is capable of measuring refractivity in the stratosphere/troposphere during the last ~30 seconds of a GPS occultation event. These refractivity observations may be converted into profiles of density and temperature. Gravity waves can be observed as fluctuations in these profiles. Thus CORISS provides insight into the source region for locally generated gravity waves that may act as “seeds” for plasma instability. Recent examinations of GPS occultation data [*Hocke and Tsuda*, 2001] have established a connection between the occurrence of stratospheric temperature fluctuations and E-region irregularities.

3.2.4 Role of Penetration Electric Fields

An important source of electric fields lies in the interplanetary medium. Through merging between the interplanetary magnetic field (IMF) and the Earth’s field, a potential difference $\Delta\Phi_{PC}$ is imposed on the polar cap ionosphere. This potential is also imposed on the magnetosphere and the global ionosphere. *Nishida* [1968] demonstrated that currents flowing in the equatorial ionosphere are affected by intensifications of the interplanetary electric field (IEF). Intensifications of $\Delta\Phi_{PC}$ increase the dawn to dusk electric field E_Y throughout the magnetosphere. This electric field causes energetic ions in the inner magnetosphere to gain kinetic energy and convect toward the Earth. As a result, the different gradient-curvature drift paths of ions and electrons begin to separate. If high values of $\Delta\Phi_{PC}$

are sustained for more than an hour, space charge builds up to shield E_Y from the innermost parts of the magnetosphere. In addition, the intensity of the ring current grows. Magnetometers at low latitudes on Earth detect decreases in the north-south component of the local magnetic field. Traces of the Dst index plotted as a function of time show positive slopes when the intensity of the ring current is increasing, and negative slopes when it is decreasing. Thus, negative slopes in Dst, dDst/dt < 0 may be regarded as a simple identifier of times when the IEF is imposing a dawn-to-dusk electric field in the inner magnetosphere, earthward of the existing ring current. ***Is dDst/dt a reliable index of incomplete shielding of the solar wind electric field, and can it be used to forecast irregularities?***

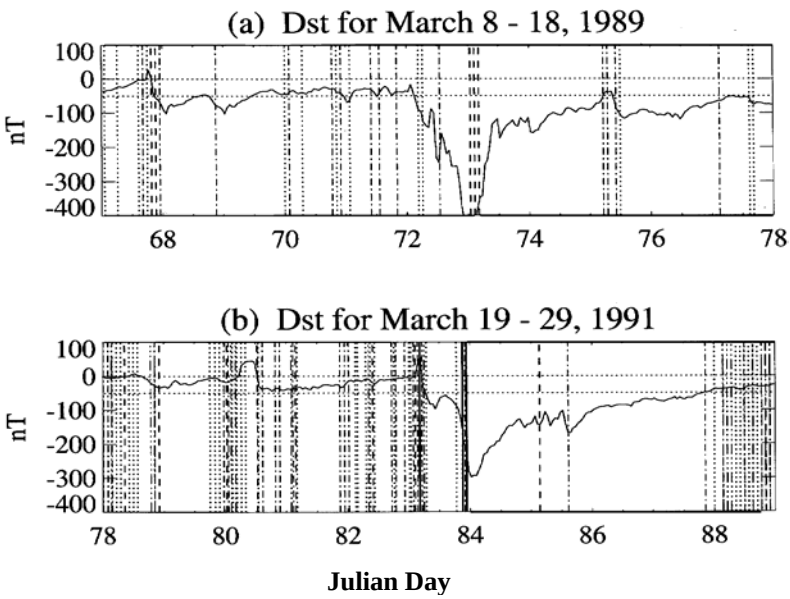

Figure 8. Dst measured near the times of two magnetic storms in (a) March 1989 and (b) March 1991 for 11 days roughly centered on the storm's maximum epoch. Vertical lines mark times of DMSP satellite encounters with EPBs. Light dotted lines, dashed lines, and heavy solid lines indicate increasing depletion severity [*Huang et al*., 2001].

3.2.4.1 Post Midnight Bubbles during Magnetic Storms

Recent studies using the Defense Meteorological Satellite Program (DMSP) satellites in the evening sector have demonstrated that EPBs occur frequently in the initial and main phases of geomagnetic storms [*Huang et al.,* 2001]. This is illustrated in Figure 8, which shows the occurrence of DMSP observations of plasma bubbles during magnetic storms. Simultaneous measurements by the Combined Release and Radiation Effects Satellite (CRRES) in the inner magnetosphere indicate that penetration electric fields were responsible for triggering the creation of these structures. During the recovery phase of almost all storms, bubbles are not detected in the evening local time sector. They are, however, evident in the post midnight to dawn local time sector. Bubble suppression in the evening sector and growth after midnight are attributed to the action of a counter dynamo driven by penetration E fields or by Joule heating at nighttime auroral latitudes [*Fejer and Scherliess,* 1997].

To take advantage of this knowledge for predicting the occurrence of EPBs, it is necessary to recognize that penetration electric fields are controlled by the variability of the IEF. ***It is desirable to establish a direct link between the IEF and electric fields in the low-latitude ionosphere.*** *Nishida* [1968] showed that the DP 2 current system responds to IEF variability. Data collected by the

Advanced Composition Explorer (ACE) satellite should be monitored to look for IEF structures that trigger EPBs. Alternately, it is possible to use the Polar Cap Index, which is a measure of DP 2 activity, to establish thresholds for bubble triggering levels. It would also be useful to compare Dst responses to IEF and solar wind pressure variations to establish criteria for predicting the end of the main and the beginning of the recovery phase of magnetic storms. This would provide an all-clear signal for communication systems to resume normal operations.

3.2.4.2 Role Of High Latitude Field-Aligned Currents

Region I and II field-aligned currents globally affect the electric field. Depending on the orientation of the zonal field at the equator, these currents can either suppress or trigger ESF and EPBs. At AFRL, this effect has been modeled by incorporating a first-order ionospheric conductivity model that includes variation in local time and latitude as well as auroral effects. The result is a numerically complex Poisson equation, which was solved numerically, yielding solutions that are consistent with previous work. Under the above assumptions it was found that Region I currents produce eastward electric fields of ~1 mV/m just eastward of the dusk terminator. The presence of Region II currents shields the equatorial region from the Region I currents and tends to suppress, if not reverse, this electric field. Therefore, the efficiency of high-latitude currents in creating and suppressing scintillations is dependent on the phase of the magnetic perturbation.

A more realistic modeling of the ionospheric conductivity needs to be incorporated into the model. Comparisons with satellite data such as that from Constellation Observing System for Meteorology, Ionosphere and Climate (COSMIC) and C/NOFS should lead to physical insights regarding the driving mechanism for the occurrence and suppression of ionospheric scintillations. It will also lead to an improved specification of the electric potential that is of magnetospheric origin. Its global distribution, as well as time evolution, will be better understood.

3.2.5 Longitudinal Ionospheric Correlation Length

C/NOFS measurements will facilitate determination of the longitudinal correlation scales of the ESF trigger or suppression mechanisms. The satellite will provide information at a given longitude every 90 minutes; the satellite footprint will advance by 22.5° during this time interval. These data, along with strategically located ground-based observations, will provide the correlation lengths. ***What controls the longitudinal correlation lengths: thermospheric or magnetospheric coupling processes? Are there other factors such as tropospheric effects or land-ocean differences?***

3.2.6 Separating Time and Longitude Effects

Ground-based observations are used to establish the time evolution of ESF and EPBs. However, some may be spatial rather than temporal structures. ***By resolving temporal and spatial ambiguities, C/NOFS may provide insights into the most important seeding mechanisms. For example, is the thermospheric wind profile more important than gravity waves or lightning?***

3.3 First-Principle Models of the Ambient Ionosphere

This section describes the planned approach for modeling and forecasting the ambient ionosphere with models that assimilate data from C/NOFS satellite and ground-based instruments. We then present a possible approach to couple time dependent models in order to forecast the state of the ionosphere through an interval of several hours. Finally, we describe a new 3D theoretical model that can be validated by C/NOFS data.

The analysis cycle of the data for forecasts is much like the cycle used in numerical forecasting of tropospheric weather: soundings from satellites provide data describing the current state of the atmosphere, which is used as an initial condition for integrating the fluid equations of motion for the atmosphere forward in time to predict the state of the atmosphere in the future. We also expect data quality control issues similar to those faced by tropospheric weather analyzers, but of particular concern is the problem of data scarcity. Furthermore, the ionosphere is dependent on external driving forces, such as the solar UV flux and the solar wind, that are much more variable and unpredictable than the drivers of tropospheric weather. C/NOFS models will rely on data that parameterize these external drivers using data from other satellites and sensors, which will be collected in the Data Center for use by the models.

3.3.1 C/NOFS Assimilation Model

The assimilation models provide a means to determine snapshots of ionosphere/thermosphere structures using data from C/NOFS and other sources. The main problem that must be addressed is data scarcity; the satellite provides only a one-dimensional sampling of the parameters needed to specify the 3D volume of the Earth's ionosphere. Other issues include recognizing data quality deterioration, nonsynchronicity of data delivery, data dropouts, and cold starts (without data).

A general description of the baseline assimilation algorithm follows. We begin the assimilation process with a predicted snapshot of an ionospheric quantity provided by an earlier run of the forecast model, or if starting cold (with no previous forecast runs or data), from an empirical specification model. In the regions where data exist (bounded by some correlation distance from the measurement points), the C/NOFS data will be used to constrain the model snapshot. The assimilation process is thus viewed as a filtering process in which, in effect, the C/NOFS data modulate the stream of data from the earlier prediction to constrain the stream to match the satellite data where the data exist, and allow the flow unaltered where the data do not exist.

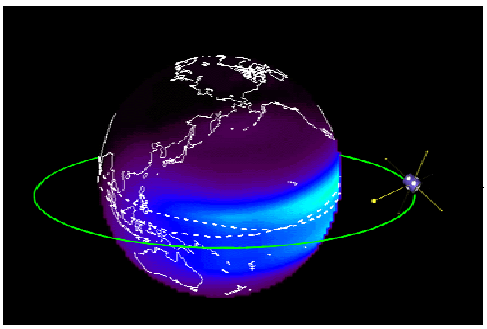

Figure 9. The satellite provides only a one-dimensional sampling of the parameters we need to specify in the 3D volume of the Earth's ionosphere. To alleviate this problem, several physical assumptions and simplifications must be made.

3.3.1.1 Electric Field Assimilation

Electric fields on several scales are significant to the C/NOFS program. One scale is global (with grid sizes of a few degrees longitude), in which the fields are predicted by the ambient dynamo model calculation. Another scale is that of equatorial plumes or bubbles, where the fields are local (over a few hundreds of kilometers) and are described by the mesoscale plasma bubble calculations. A low-pass filter on the field data will enable us to separate the different scales so we can assimilate the global-scale fields for use in the ambient model. To help achieve coverage of the ionospheric volume, geomagnetic field lines will be regarded as equipotentials at the relevant spatial scale (see Figure 9).

A vector measurement of the electric field at one point by the satellite thus provides the electric field at all points along the geomagnetic field line that intersects the observation point. As the satellite sweeps through its orbit, it measures the fields through the whole range of longitudes or local times. ***A model is required, however, to specify the variation of the fields through the third dimension, field-line apex altitude. Can the predicted fields from the previous forecast be used as the prescription of the variation of field with altitude?***

Shorter-scale electric fields in the vicinity of the bubbles will be used to describe the movement of these structures. ***Can bubble velocity be used to predict how the bubbles will drift, and thus provide a short-term forecast of the location of scintillations? Will vertical plasma drifts within the bubbles indicate how high they will rise, and thus to what latitudes their turbulence effects will be seen?***

3.3.1.2 Ion Density Assimilation

Gradients in the ion density in the bottomside of the ionospheric F layer are strong determinants of the plasma's vulnerability to the R-T instability. Unfortunately, the satellite will rarely be flying in this region, so we will be unable to measure bottomside gradients directly. The height of the bottomside gradient, however, strongly depends on the vertical velocity of the plasma, which is determined by electric fields. Latitudinal gradients in the plasma density are controlled by the interhemispheric neutral winds. The data that will be assimilated to prescribe the ion density are the electric field, neutral wind, and the local ion density at the satellite observation point. ***What will be the accuracy of the EDP values calculated by the assimilative models?***

Outside the unstable region, we still need an accurate ion density model to help specify the propagation of high-latitude phenomena which drive the variable neutral winds and dynamo fields at the equator. We can take advantage of the worldwide network of GPS sensors measuring TEC that is operated by the Jet Propulsion Laboratory and assimilate these data as well as data from the AF operational network of ionosondes stations into the PRISM model to specify the ion density at mid and high latitudes.

3.3.1.3 Thermospheric Assimilation

Data from the NWM will be assimilated to specify the winds. ***Can the variability of these dynamo winds explain the variability of the vertical plasma drifts that cause the variability of EPB occurrence?*** Here the plan is to constrain by the measured wind the output of the standard climatological model, the Hedin Wind Model [*Hedin et al., 1988*], and then use the constrained model to provide the full 3D wind specification. There will be no neutral pressure, density, or temperature sensors on the C/NOFS satellite, so empirical models will specify these parameters.

3.3.1.4 Assimilation of GPS Occultation Data

The assimilation of CORISS GPS occultation observations is more complex than the assimilation of *in situ* observations, primarily because of the comparatively complex observational geometry associated with the GPS occultation technique. For this reason, assimilation of the CORISS data will not be done during the initial phase of the C/NOFS project. However, there are several significant benefits that may accrue from eventual use of these data. In particular, EDPs derived from CORISS should provide a measure of the height of the maximum in the bottomside vertical gradient and of E-region densities. The C/NOFS *in situ* ion sensors cannot estimate these quantities. Algorithms to extract these parameters from CORISS ionospheric profiles will have to be developed and tested prior to using these data in an assimilative scheme. These algorithms will have to compensate for the effects of horizontal gradients on CORISS profiles. CORISS slant path TEC observations of both northern and southern arcs may also provide sufficient information to constrain specification of neutral winds for modeling purposes under some conditions. This would be particularly useful during

times (i.e., apogee) when the C/NOFS satellite is too high for the *in situ* neutral wind sensors to operate effectively.

3.3.2 Ionospheric Forecasting

3.3.2.1 Ambient Forecast Model

The forecast of the ambient ionosphere begins with a snapshot of the ionosphere provided by the assimilation process and advances it through the forecast interval. This model provides global coverage of both the plasma constituents and neutral thermospheric components of the ionosphere through the range of heights relevant for ionospheric processes, at a horizontal resolution of a few degrees in latitude and longitude. One approach is to couple a set of familiar models for the components of the ionospheric/thermospheric system in a self-consistent way as illustrated in Figure 10 and as described below.

External Drivers: There are several external forces with great influence on the behavior of the ionosphere including the solar UV flux, for which we use the Hinteregger reference spectra as an empirical specification model. This model is parameterized by the solar radio flux index, F10.7. At high latitudes, auroral precipitation is another source of heat and ionization. Penetration electric fields are just one of the ways in which magnetospheric processes can affect the low latitude ionosphere [Scherliess and Fejer, 1997]. These fields will be incorporated into the model using empirical models driven by data from the ACE satellite and/or geomagnetic activity indices.

Thermospheric Forecast Model: The Thermospheric Forecast Model (TFM) of *Fuller-Rowell and Rees* [1981] solves the nonlinear continuity, momentum, and heat equations for the neutral constituents of the thermosphere. Given an initial specification of horizontal winds on pressure surfaces, these equations are integrated forward in time to describe the evolution of the winds and composition. Required inputs include the solar UV flux, low-altitude tidal amplitudes, and the ion densities and drifts around the globe. TFM can describe several phenomena including the diurnal variation due to solar heating, various planetary waves, and the response of the atmosphere to geomagnetic activity.

Mid- and High- Latitude Plasma Model: The plasma forecast model solves the nonlinear continuity equation for the evolution of the ion density as a function of time and space given an initial density distribution, the velocity field as a function of time and space, and the various processes that describe plasma sources and loss rates. Space Environment Corporation's Ionospheric Forecast Model (IFM) includes a mid- and high- latitude code in addition to its low-latitude plasma code which describes the detail of the plasma structure.

Low-Latitude Plasma Forecast Model: The low-latitude plasma forecast model performs the same function as the mid- and high- latitude model, but for the plasma near the equator. Because the plasma flow is intimately tied to the geometry of the geomagnetic field lines and the geometry is different in the two regions (field lines that close within the simulation volume versus field lines that do not), a separate code is devoted to the low latitude. The choices for this code in the system are all descendants of *Anderson* [1973] LOWLAT code. One is the low-latitude code in IFM; the other is the updated version of LOWLAT found in Geolib [Retterer, private communication]. The plan is to use IFM because it has been validated for operational use. The IFM code is available in several versions; in addition to its IFM implementation, there is the regional version, LLIONS [*Schunk et al., 1997*] and the assimilative version, RIFS, which we will be using in the assimilation of C/NOFS data.

Conductivities, Currents, and Dynamo Model: Assuming that the global electric field is electrostatic in nature, the equation of current continuity gives us an elliptic equation for the electric potential in terms of the field-line integrated plasma conductivities and currents driven by neutral winds and other forces. Given plasma and neutral densities, temperatures, and drifts, the conductivities and current

densities are simply evaluated using standard formulas, and then the elliptic equation can be solved for the electric potential, given boundary conditions derived from the mid-latitude electric potential. The dynamo model of *Eccles* [1998a], which is coupled to IFM, is the prime choice of model here.

To conclude, the forecast of the global ionospheric density will constitute a major scientific challenge. ***Do these models include all the appropriate physics? How far into the future will the simple extrapolations of the drivers allow us to forecast?***

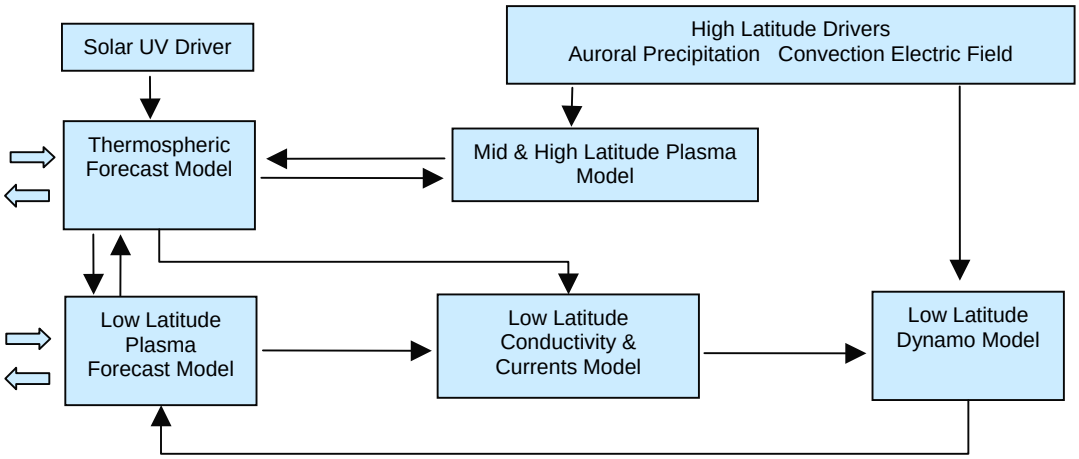

Figure 10. The C/NOFS ambient ionosphere forecast model. Models for several constituents of the ionosphere/thermosphere system are coupled to provide a forecast.

3.3.3 Global 3D Modeling Using SAMI3

C/NOFS observations can also be used to validate a 3D physics model that has recently been developed at NRL, SAMI3 *[Huba and Joyce, 2002]***.** The model treats the dynamic evolution of seven ion species (H^+, He^+, N^+, O^+, N_2^+, NO^+, and O_2^+) in the altitude range 85 - 18,000 km. Thermal balance equations are solved for three ion species (H^+, He^+, and O^+) and the electrons. The model uses an offset, tilted dipole approximation to the geomagnetic field and solves the continuity, momentum, and thermal equations along the field from hemisphere to hemisphere. The neutral atmosphere is specified using empirical codes.

SAM13 uses a non-uniform, non-orthogonal grid transverse to the geomagnetic field. The model includes ion inertia parallel to the geomagnetic field, as well as the radial and longitudinal E x B transport of the plasma. A time-splitting scheme is used: the dynamics of the system is first solved for motion along the geomagnetic field and then for motion transverse to the geomagnetic field. The motion of the plasma along the geomagnetic field is described by a set of advection/diffusion equations.

Three key aspects of SAMI3 make it attractive for modeling ESF. First, it is a fully 3D model. Second, it uses a grid that can be tailored to model spread F (for example, the longitudinal non-uniform, non-orthogonal grid can be refined in the local sunset sector to capture ESF behavior on length scales of the order of tens of kilometers). Third, the numerical scheme follows the plasma transport on short time scales (few seconds), as needed for spread-F modeling.

4 Triggering and Suppressing Equatorial Plasma Instabilities

An important component of the C/NOFS science plan is to identify the ionospheric conditions that lead to the onset of plasma instabilities and to understand the aspects that act to suppress the onset. This will enable us to forecast the timing and the severity of ESF activity.

4.1 Role of Wind Shear and Vertical Wind Variations

Recent theoretical and numerical simulation studies have indicated that, in addition to gravity and the eastward electric field just after sunset, the sheared horizontal neutral wind velocity can also control the excitation of plasma instabilities.

The zonal neutral wind is at a maximum at the magnetic equator and is at a minimum at the crests of the equatorial anomaly because of ion drag [*Raghavarao et al.,* 1991]. The neutral temperature is also enhanced at the crests of the anomaly and is at a minimum at the magnetic equator. This phenomenon has been termed as the equatorial temperature and wind anomaly. The empirical Hedin Wind Model [*Hedin et al*., 1988] does not reproduce the latitude variation of neutral winds. The variation of neutral wind and ion motion with magnetic latitude results in a vertical shear of zonal neutral wind at the magnetic equator [*Anderson and Mendillo,* 1983; *Raghavarao et al.,* 1991]. The shear has been shown to be responsible for the tilt of plume structures, which is eastward at lower altitudes and westward at higher altitudes [*Zalesak et al.,* 1982]. The role of shear in the stabilization of the R-T instability causing the generation of irregularities over a narrow confined altitude, called bottomside spread F, has also been investigated [*Sekar and Kelley,* 1998].

The enhanced neutral temperature recorded by the DE-2 satellite at the crests of the equatorial anomaly may set up a circulation cell in the meridional plane causing vertically downward winds at the magnetic equator [*Raghavarao et al.,* 1993]. Such vertical winds contribute towards increasing the growth rate of the R-T instability.

In addition to the zonal and vertical neutral winds, there is a trans-equatorial flow from the summer to the winter hemisphere in the early evening and late night hours with essentially zero velocities in between [*Biondi et al.,* 1991]. At the equinoxes, an early evening poleward flow at solar minimum is replaced by an equatorward flow at solar maximum. The meridional neutral winds can cause an asymmetric ionization distribution in the equatorial anomaly that can lead to an increase in the F-region Pedersen conductivity and a decrease in the growth rate of the R-T instability. A hypothesis was put forward to suggest that the day-to-day variability of ESF might be related to the presence or the absence of meridional neutral winds [*Mendillo et al.,* 1992]. However, recent simultaneous measurements of meridional neutral winds and nighttime equatorial irregularities could not establish the spread F suppression role of meridional neutral winds [*Mendillo et al.,* 2001].

For these reasons, an important set of science objectives is to address the role of wind shear in the formation of irregularities and to determine if the asymmetry in the Appleton anomaly is a good scintillation predictor.

4.2 Effects of Plasma Inhomogeneities

The ionospheric plasma parameters, which determine the onset and growth of plasma instabilities, are highly variable both spatially and temporally. In spatially nonuniform plasma, a topological requirement for the onset of plasma instabilities is that the plasma modes have localized spatial profiles that are consistent with the physical regimes in which they are excited and that they grow over the region of localization on realistic time scales without convecting. In the equatorial

ionosphere, the spatial variation of the electrical resistivity along the curved dipole magnetic field lines and that of density and ion-neutral collision frequency along the vertical direction help in realizing the localized modes [*Basu and Coppi*, 1983; *Basu and Coppi*, 1999]. On the other hand, the spatial variation of other plasma parameters can impose severe constraints that make the excitation of plasma modes topologically unfavorable, and so the instability may be inhibited [*Basu and Coppi*, 1999]. ***First-principles theoretical models will assist us in gaining quantitative understanding of the effects of inhomogeneities of various ionospheric parameters on the plasma instability mechanisms.*** This, in turn, will determine which plasma parameters have more influence than others on the onset of the instability and so should play a more important role in the forecasting models.

Spatial profiles of the ionospheric plasma parameters are essential inputs for the study. Rocket measurements in coordination with the C/NOFS satellite measurements and other available ground-based (e.g., radar, ionospheric sounder) measurements will be useful in validating the concept and the models based on it.

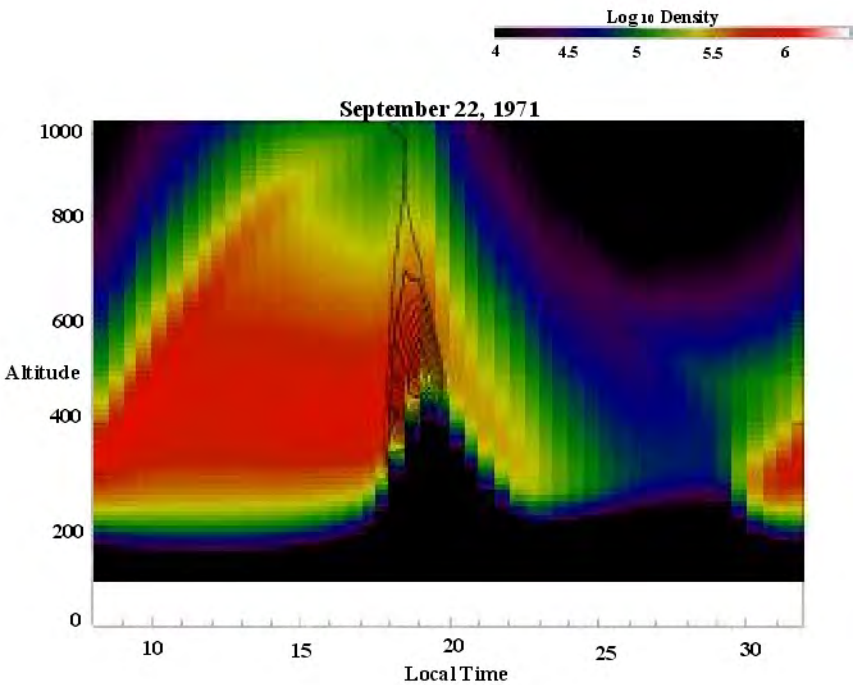

Figure 11. Plasma density obtained from the assimilation of observed vertical drifts into the low-latitude ionosphere model. The September 22, 1971 data are plotted as a function of altitude (km) and local time. Superimposed on the plot are the contours of R-T growth rate spaced at increments of 2.5×10^{-4} s^{-1}, beginning with the outermost contour for a growth rate of 7.5×10^{-4} s^{-1}, and increasing inward.

4.3 Linear Growth Rate Model

An important component of the C/NOFS science plan is to develop a theoretical model that accurately calculates the linear growth rates by incorporating the pertinent plasma inhomogeneity effects. The linear growth model is needed to specify and forecast where in the equatorial ionosphere bubbles and plumes may occur with high probability. Presently, a flux-tube integrated description of the equatorial plasma instability, introduced by *Haerendel* [private communication, 1973], is used to

calculate the linear growth rates. Such a description takes into account the effects of plasma inhomogeneity, but makes several simplifying assumptions. An accurate theoretical model must address the plasma inhomogeneity effects discussed above by adopting a more rigorous mathematical description. AFRL has developed such a model (see Figure 11), but it needs to be extended and validated using C/NOFS. Once again, spatial profiles of the ionospheric plasma parameters are essential inputs for the model, and coordinated rocket measurements will be useful.

C/NOFS instruments will measure many of the parameters needed to specify the ambient ionosphere and to forecast which regions will be susceptible to plasma instabilities. Because there are a variety of different assumptions which can be made when performing a linear instability analysis of the ionospheric plasma, correlations of the theoretical predictions of possible models with the observed occurrence of bubbles will be important in discriminating between the models and identifying the set of assumptions which best characterize the conditions under which plasma perturbations grow.

C/NOFS measurements will also provide insights into the seeding or preconditioning of the plasma for the conditions that permit the instabilities to occur. Much like the Atmospheric Explorer-E observations of sizeable gravity waves in which plasma bubbles were found to form in the troughs [*Singh et al.*, 1997], C/NOFS observations of the ionosphere and thermosphere prior to the formation of bubbles will provide insight into the processes and conditions preceding bubble onset.

4.4 Cascading Processes

EPBs are plasma-depleted flux tubes that extend many tens of kilometers in longitudinal width and thousands of kilometers in latitudinal length. EPBs generally originate in the bottomside of the F layer at post sunset local times, except during extended periods of geomagnetic activity.

Spectral analysis of measurements obtained in rockets flying through ionospheric bubbles suggests that the turbulent plasma contains significant structure over an astonishing range of wavelengths: from hundreds of kilometers down to meter wavelengths and smaller. Over a fair portion of this wavelength range, the spectrum of density fluctuations has a regular, power-law-like form.

What is the cascading process that is effective for the transfer of spectral power between wavelengths? By analogy with neutral turbulence, we call the power law regime one of energy cascade. There are several candidates for the mechanism of this cascade process, including wave steepening as well as excitation of drift waves and other secondary plasma instabilities. However, the paucity of data (there have been only a few rocket missions through bubbles) has prevented the mechanism (or mechanisms) from being identified with authority. C/NOFS will be flying through bubbles frequently throughout its mission with plasma density and electric field instruments to sample the density structures and the electric fields within and near the bubbles.

The electric field instrument, VEFI, is being designed to specify many of the characteristics of the plasma turbulence. VEFI will measure quasi-DC electric fields at rates of up to 2048 samples per second. A filter bank and a digital signal processing system will permit measurements of higher frequencies. The boom system can be used as an interferometer, permitting determination of the phase velocities of waves. The plasma density instrument, PLP, is also designed to sample at kHz frequencies to allow resolution of structures on the scale of meters. These measurements will enable us to identify the electrostatic plasma waves that mediate the cascade process. In addition, a 3-axis magnetometer, which is also part of the design, will provide magnetic-perturbation signatures of the bubbles when they move at hyper-Alfven velocities. These have been observed occasionally before. Such signatures will indicate whether or not electromagnetic waves are also candidate mechanisms for the cascade process. The irregularities associated with the cascade process and spread F in general are discussed in more detail in Section 5.

In addition, given the δE and δB, it is possible to measure the magnitude and direction of the Poynting flux in spatial structures. This in turn yields the overall Σ_P in the off-equatorial E region.

4.5 What is the Bubble Spatial Structure?

The standard theory predicts that EPBs will be aligned with the geomagnetic field. However, they often show bifurcations and irregular shapes. As an example, Figure 12 illustrates a fully developed structure in an image taken from the AF facility at the top of the Haleakala volcano. The emission is from the 777.4 nm oxygen recombination line. The airglow depletions are very turbulent and map along field lines to locations north of Hawaii. Severe scintillations accompany the signatures that can be seen in the lower panel, which shows the S_4 index from the GPS data taken in Hawaii.

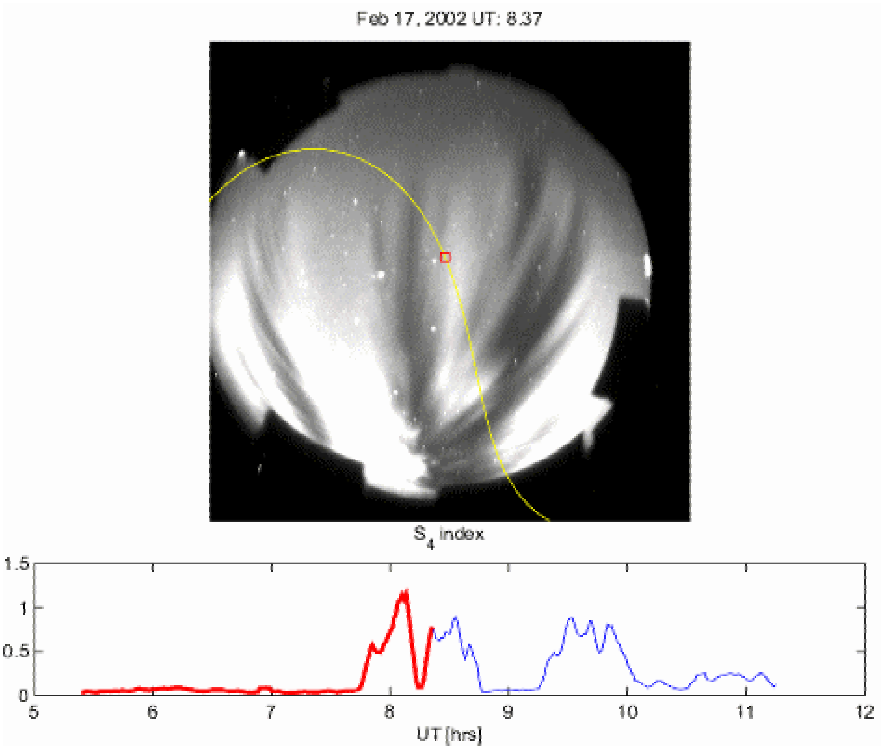

Figure 12. Haleakala all-sky camera (ASC) image and GPS scintillations. Severe scintillations, as shown in the lower panel by the S4 index from the GPS data, correlate to depleted regions of electron density (upper panel). S4 index history shows scintillations occurred before the camera was turned on at 2020 LT. The GPS orbit is shown on the ASC image.

Because of the tilt between the geomagnetic field and the C/NOFS satellite's low earth orbit, the satellite will sample ionospheric bubbles at a variety of positions along their latitudinal extent, as well as at a variety of altitudes and local times. Thus, these data, as they accumulate over time, will give us a statistical picture of the structure of EPBs. We will be able to resolve the following questions:

- ***How buoyant are the bubbles in the ionosphere (and thus how high will they rise)?***
- ***How far along the geomagnetic field lines do they extend?***